

## Western Pacific Moisture Analysis as Observed from DMSP SSM/I Measurements

HUO-JIN HUANG<sup>1</sup>  
GIN-RONG LIU<sup>2</sup>, and TANG-HUANG LIN<sup>2</sup>

(Received: September 15, 1992; Revised: December 5, 1992)

### ABSTRACT

DMSP SSM/I data are used in this study to investigate the global distribution of moisture, and to study the variations of brightness temperatures with the changes of the intensity of typhoons during September 1987. The rain rate of typhoons is also determined based on Olsón *et al.*'s (1990) algorithm.

It is noted that the SSM/I data could provide realistic patterns and magnitudes of total precipitable water, cloud water content, and rain rate for the globe. They are comparable to the previous findings and other model analysis. The characteristics of SSM/I data are documented in this study for the three typhoons (Gerald, Freda, and Holly) over the western Pacific Ocean. The detailed structure of the typhoon can be identified by the SSM/I data, and the estimated rainfall of the typhoon appears to be reasonable.

The development of the algorithms to derive atmospheric variables for Taiwan and its vicinity is suggested, and the validation of the algorithms has to be executed based on radar data, and upper and surface observations. The intercomparisons of various algorithms also can be performed, if ground truth data are not available.

### 1. INTRODUCTION

Remote sensing measurements from satellites have facilitated studies of atmospheric moisture and tropical cyclones for almost three decades. Early remote sensing research focused on the use of visible and infrared data to investigate the cloud coverage and patterns, surface variables, vertical profile of temperature, and to determine rainfall and convection intensity.

The microwave channel data became available since the beginning of the Nimbus series satellites in 1972. They have been providing global coverage of good quality of various

---

<sup>1</sup> Department of Atmospheric Sciences, University of North Carolina at Asheville; Visiting Associate Professor of Center for Space and Remote Sensing Research, National Central University

<sup>2</sup> Center for Space and Remote Sensing Research, National Central University

estimated atmospheric and surface variables, such as total precipitable water, cloud (liquid) water content, rainfall, surface wind speed, and surface temperature. Several specialized field experiments have also been conducted to validate the algorithms that determine the values of these variables. Previous studies have shown that the passive microwave method could provide realistic global patterns of moisture. Researchers have also found that the intensity of tropical cyclones and evolution of midlatitude cyclones can be determined accurately by using various algorithms based on microwave data.

The higher microwave frequencies with better resolution aboard satellites were not available until the launch of DMSP (Defense Meteorological Satellite Program) F8 satellite on June 19, 1987; that was equipped with the Special Sensor Microwave/Imager (SSM/I). SSM/I offers a data set of unprecedented quality and temporal coverage to study global distribution of moisture and tropical cyclones.

The present study's purpose is to use DMSP F8 SSM/I data to investigate the global distribution of moisture, and to study the intensity and rainfall of three typhoons over the western Pacific Ocean during September 1987. The objective is to promote the understanding of the characteristics of microwave data, and to initialize the future research on the applications of microwave data.

## 2. PASSIVE MICROWAVE MEASUREMENTS

At microwave frequencies, remote sensing instrument can "see" through clouds to observe surface features with rain (large liquid and ice hydrometers) being the major source of variations; the surface features (such as sea ice, snow cover, ice type, surface wind speed, roughness of ocean surface, vegetation covers, and others) can be determined adequately and accurately. Most moisture variables in the atmosphere, such as total precipitable water, cloud (liquid) water content, and rainfall intensity can also be derived using various algorithms. However, most atmospheric variables can only be determined over oceans, where the background brightness temperatures are nearly constant. The low emissive brightness temperatures are distinct from the brightness temperatures of clouds and precipitation.

For the microwave frequencies below 37 GHz, rain may be evidenced by the greater brightness temperature due to increased emission of the liquid and ice hydrometeors; while above 60 GHz, rain can be detected by decreased brightness temperature due to the scattering by ice hydrometeors. At frequencies between 37 and 60 GHz, the combination of both emission and scattering prevails.

Large raindrops and ice particles, such as graupel or hail, scatter microwave radiation, effectively lowering the background brightness temperature by scattering emitted radiation away from the satellite. This effect is most pronounced at high frequencies at which the particle size hydrometeors are equally effective over water and land. More detailed review on the passive microwave measurements is discussed in Huang and Liu (1992).

The relationship, though indirect, between this scattering process and surface rain rate, enables the SSM/I 85.5 GHz observations to play a key role in identifying precipitation. This capability has already been shown by using aircraft microwave data at 92 GHz (Wilheit *et al.*, 1982; Harkkarinen and Adler, 1988; Heymsfield and Fulton, 1988), by analysis of coupled radiative transfer/numerical cloud models (Adler *et al.*, 1988), and by analysis of SSM/I data (Spencer *et al.*, 1989). This relationship can also be seen in the calculations of Wu and Weinman (1984).

### 3. DMSP SSM/I DATA

On June 19, 1987, Special Sensor Microwave/Imager (SSM/I) was launched aboard the Defense Meteorological Satellite Program (DMSP) block 5D-2 Spacecraft F8. The DMSP orbit is circular, sun-synchronous, and near-polar, with an altitude of 833 km and an inclination of  $98.8^\circ$ . The orbit period is 101.42 minutes (about 14.1 orbits per day). The local times for the ascending and descending equatorial crossing are 6:12 am and 6:12 pm, respectively. The orbit provides complete coverage of the earth, except two small circular sectors of  $2.4^\circ$  centered on the North and South poles. Table 1 lists the orbital parameters of DMSP.

The DMSP SSM/I has actually 7 separate total-power radiometers, each simultaneously measuring the microwave emission coming from the earth and the intervening atmosphere. Dual polarization measurements are taken at 19.35, 37.0, and 85.5 GHz, and only vertical polarization is observed at the 22.235 GHz water vapor channel. The spatial resolutions of these channels vary from about 15 km (85.5 GHz) to 60 km (19.35 GHz) depending on the frequency. Table 2 summarizes the characteristics of SSM/I.

Each observation is taken during a  $102.4^\circ$  segment of the rotation when the SSM/I is looking in the aft direction, as is shown in Figure 1. The  $102.4^\circ$  arc is centered on the spacecraft subtrack and corresponds to a 1394 km wide swath on the earth's surface. During each scan, the 85.5 GHz channels are sampled 128 times over the  $102.4^\circ$  arc. The integration period for a single sample is 3.89 ms. This sampling scheme results in 128 vertical polarization footprints and 128 horizontal polarization footprints having an effective 3-dB resolution of about 15 km for 85.5 GHz channels. A more detailed description of the SSM/I can be found in Hollinger *et al.* (1987) and Huang and Liu (1992).

The coverage of SSM/I is far better than its predecessor, SMMR (Scanning Multichannel Microwave Radiometer) on Nimbus-7 and Seasat satellites. The mosaics of all 14 ascending and descending swaths in one day are shown in Figure 2. It should be noted that these swaths are asynoptic (not synoptic). Each swath is 101.42 minutes before or after the neighboring swaths, and the last swath of the day can be almost 23.5 hours after the time of the first swath of the day. The first swath of the day is to the west of the last swath of the day by  $25.4^\circ$  longitudes. The diamond-shaped gaps in one day are centered at about  $20^\circ$ N and  $20^\circ$ S. This coverage is adequate for global- and synoptic-scale studies, especially as the average of a few days is desired. Nevertheless, the temporal resolution may not be sufficient for meso-scale research.

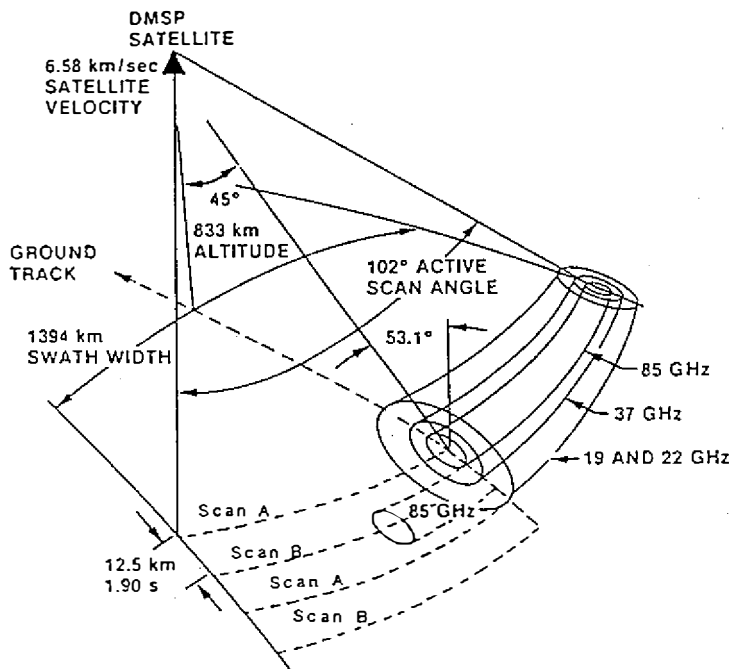
On the average the intersections of ascending and descending nodes are about 780 km apart; they become much closer together as latitude increases, until they are 220 km apart for the most poleward intersections. This pattern migrates westward and nearly repeats at six-day intervals. The 1394 km swath width gives daily coverage of the equator, double coverage (i.e., twice daily) for half of the subtropics, and quadrupled coverage poleward of about  $60^\circ$ N and  $60^\circ$ S.

Table 1. Orbital characteristics of DMSP F8.

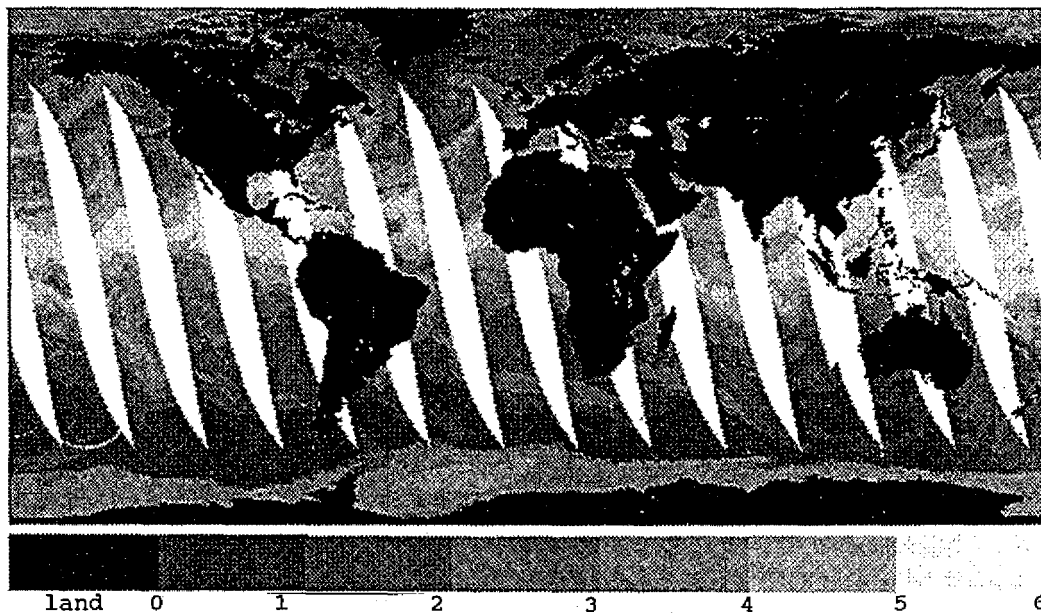
Launch date	19 June 1987
Orbit type	Near circular, sun-synchronous,
near polar orbiting	
Satellite altitude	833 km
Satellite velocity	6.58 km/s
Orbital period	101.42 minutes (6085.3seconds)
Inclination angle	$98.7^\circ$
Approximate repeat cycle	6 days (85 orbits)
Cross-equator time	6:12 am (ascending) and 6:12pm(descending) local time

Table 2. SSM/I characteristics.

Duty cycle	Everyday			
Radiometer type	Total power			
Feed-antenna relation	Synchronously rotating once in 1.9 seconds			
Scan type	Continuous rotation			
Active scan angle	102.4°			
Earth incidence	53.1°			
Center frequency (GHz)	19.35	22.235	37	85.5
Center wavelength (cm)	1.550	1.349	.811	.351
Polarization	V, H	V	V, H	V,H
On-orbit delta-T (°C)	0.7	0.4	0.8	0.4
Field of view (integrated 3 dB limits, km)	70X45	60X40	38X30	16X14
Swath width (km)	1394	1394	1394	1394
Integration time (ms)	7.95	7.95	7.95	3.89
Spatial sampling (km)	25	25	12.5	12.5
Temporal sampling (seconds)	3.80	3.80	3.80	1.90

Fig. 1. Scan geometry of SSM/I (after Hollinger *et al.*, 1987).

SSM/I Total Precipitable Water (g/cm<sup>2</sup>) Ascending 9/2 1987



SSM/I Total Precipitable Water (g/cm<sup>2</sup>) Descending 9/2 1987

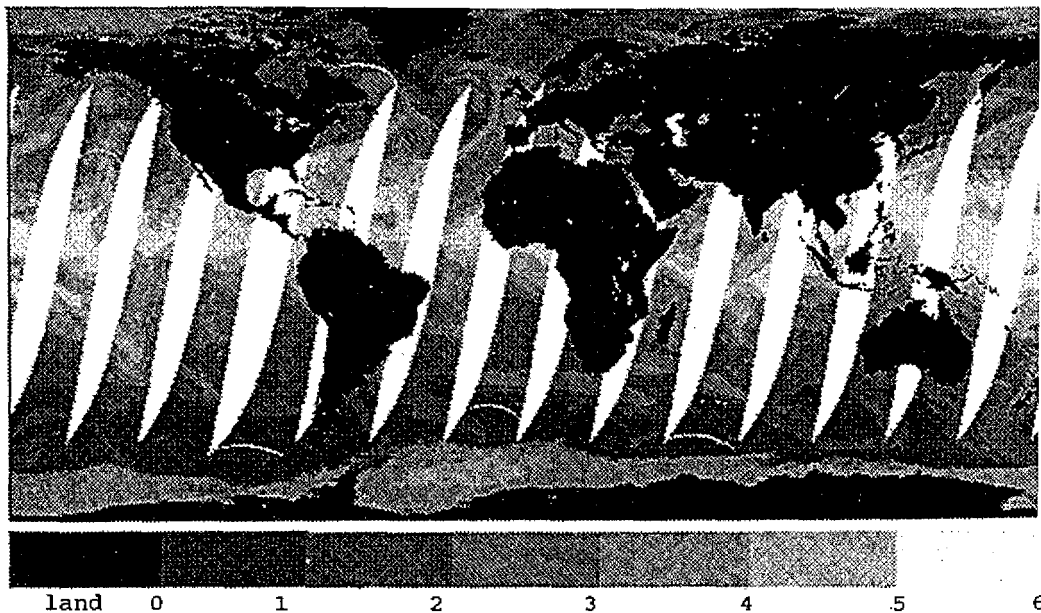


Fig. 2. Mosaics of SSM/I ascending (upper panel) and descending (lower panel) swaths of September 2, 1987.

#### 4. GLOBAL DISTRIBUTION OF MOISTURE

The global distribution of moisture is studied for August 31-September 27, 1987. This period is further divided into two 14-day periods, namely, August 31-September 13, and September 14-27, 1987, respectively. The estimated variables are the total precipitable water, cloud (liquid) water content (both are based on the algorithms of Alishouse, 1983), and rain rate as estimated by Olsón *et al.* (1990).

In the first period (August 31-September 13), three typhoons (Gerald, Freda, and Holly) occurred almost at the same time over the western Pacific Ocean. The detailed analysis of these typhoons will be discussed in Sections 5 and 6. In the second period (September 14-27), it represents a tranquil state over the western Pacific Ocean.

The SSM/I data obtained from the NASA WetNet program are in image format with brightness temperatures at pixels. Each global composite image is 640 (called elements or columns) by 320 (called lines or rows) pixels, and full resolution swath of brightness temperatures is 128 (elements or columns) by 1610 (lines or rows) pixels. The image data are processed in the PC-McIDAS (Personal Computer-Man-computer Interactive Data Access system) software package, that was developed by the Space Science and Engineering Center of the University of Wisconsin-Madison, Wisconsin. The digitalized pixel values are transferred to the VAX microcomputer at the Center for Space and Remote Sensing Research (CSRSR), National Central University to perform statistical analysis, because PC-McIDAS limits the pixel values to between 0 and 255. All negative values will be considered as zero, and all values more than 255 become 255.

The average of variables of all the ascending and descending swaths for the studied period yields the mean state. The standard deviation is the square root of sum of squares of deviation (difference between daily values and mean state) divided by number of occurrences minus 1. It represents daily variations of the weather systems. The final products are converted back to PC-McIDAS for displaying and checking, and eventually to ERDAS image processing software at CSRSR for making hard copies.

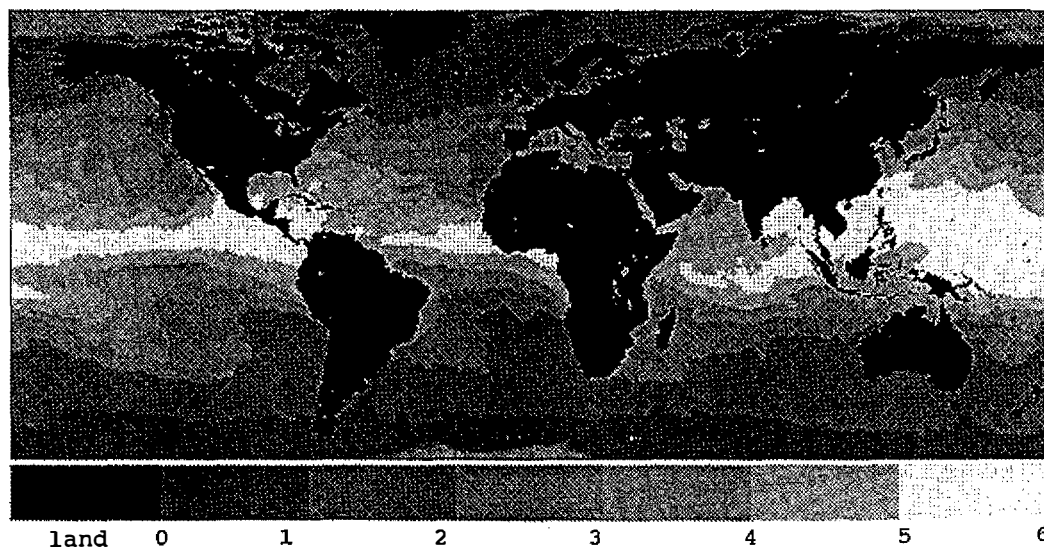
Figure 3 shows the mean and standard deviation of total precipitable water of the first period between 60°S and 80°N. Tropical moisture in the Pacific maximizes west of the dateline, and extends along the equator into the Indian Ocean, Atlantic Ocean, and the eastern Pacific Ocean. This high concentration of moisture coincides with the ITCZ (InterTropical Convergence Zone). The extension of moisture maximum intruding from the east of dateline into the Southern Hemispheric midlatitudes characterizes the SPCZ (South Pacific Convergence Zone), whose counterpart over the South Atlantic Ocean, the SACZ (South Atlantic Convergence Zone), is inactive during this period. The drier air over the high latitudes is noted for its cold temperature.

By comparing Figure 3 to the monthly means of total precipitable water of September 1987 as analyzed by NMC (National Meteorological Center) and ECMWF (European Centre for Medium-range Weather Forecasts) (see Figure 4), we found striking quantitative similarities. SSM/I estimates, however, show more details than those of NMC and ECMWF.

The moisture variability at the time scale of transient features can be studied in the standing deviation of daily SSM/I to the 2-week mean. Transient activity maximizing east of the midlatitudinal continents clearly identifies middle latitude storm tracks. The largest variability exists east of Japan, but significant fluctuations extend across the north Pacific to 150°W. The presence of synoptic transients in the SPCZ and SACZ is also apparent. The high variability over northern Australia signifies the migrating cyclones in this region. As for the local maximum off Baja, California, it is possibly caused by the variabilities of fog and low stratiform clouds in this region. The small variability of moisture over the ITCZ is also noted as expected.

The mean and standard deviation of cloud (liquid) water content of the same period are presented in Figure 5. Because condensation often occurs in convective towers and mesoscale systems, it is expected that cloud (liquid) water content would show more small scale details than the total precipitable water as illustrated in Figure 4. Narrow concentrations of cloud

SSM/I Total Precipitable Water (g/cm<sup>2</sup>) 8/31 - 9/13 1987  
Mean



Standard Deviation

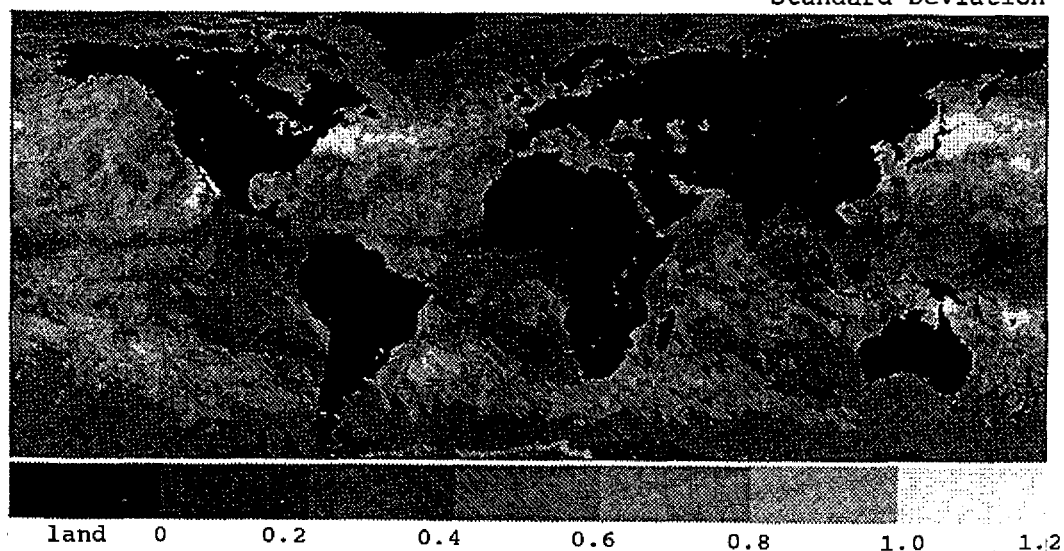


Fig. 3. Global distribution of mean and standard deviation of total precipitable water (g/cm<sup>2</sup>) for August 31-September 13, 1987.

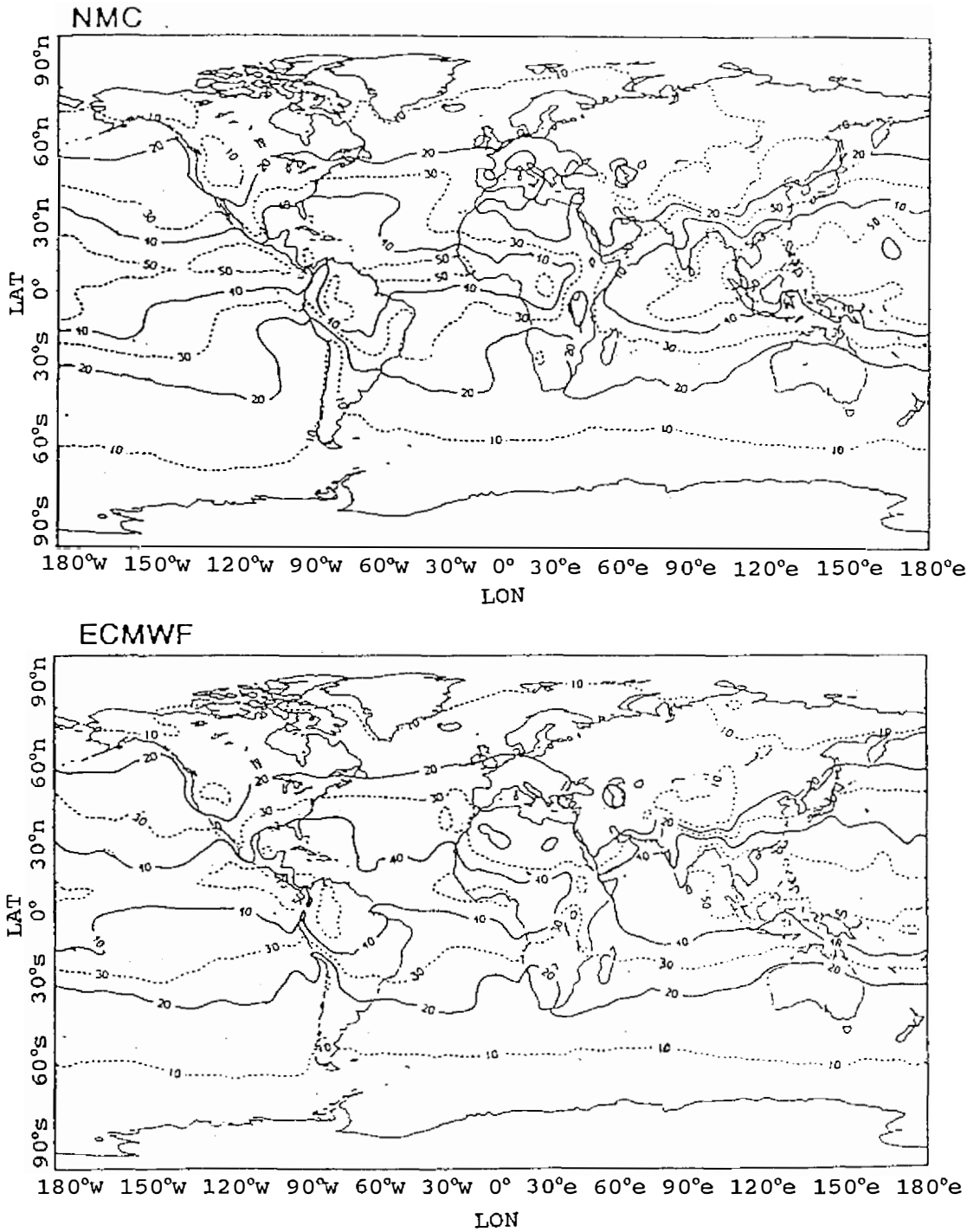
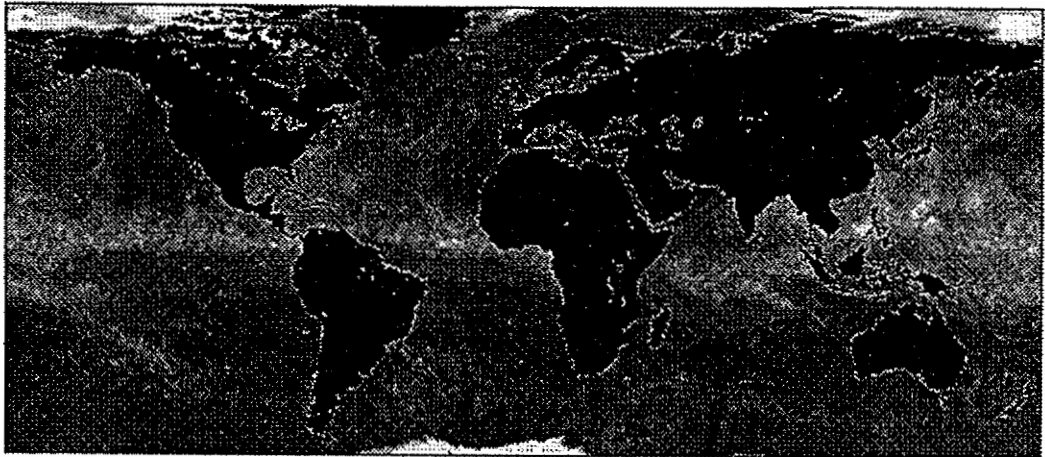


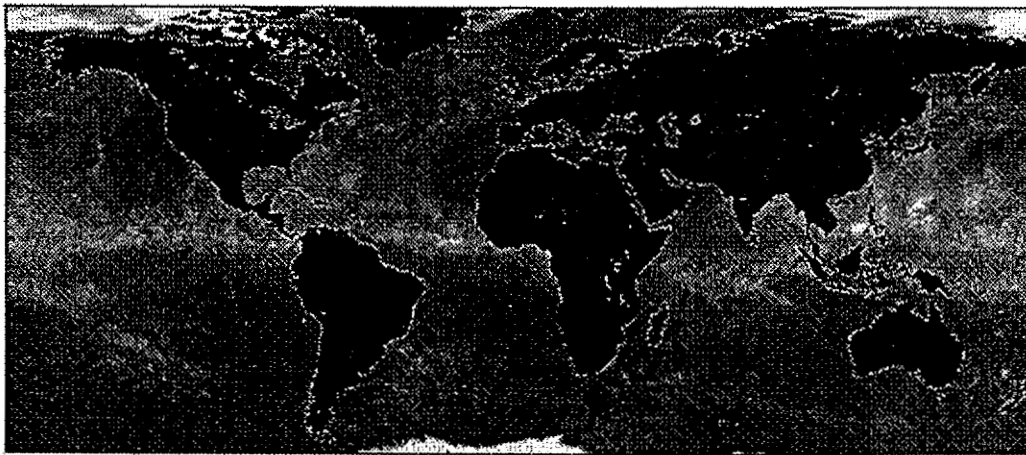
Fig. 4. Global distribution of monthly mean of total precipitable water (mm) of September 1987 as determined by NMC and ECMWF (after Robertson and Huang, 1989).

(liquid) water content along the ITCZ and SPCZ are noted. The convection associated with extratropical cyclones is also identified. The maxima over the western Pacific Ocean clearly show the tracks of three typhoons, namely, Gerald in the west, Freda in the middle, and Holly in the east. The standard deviation of liquid water content is very similar in pattern and has values smaller than the 2-week mean.

SSM/I Cloud Water Content (mg/cm<sup>2</sup>)8/31 - 9/13 1987  
Mean

land 0 10 20 30 40 50 60 70

Standard Deviation



land 0 10 20 30 40 50 60

Fig. 5. Global distribution of mean and standard deviation of cloud water content (mg/cm<sup>2</sup>) for August 31-September 13, 1987.

Figure 6 shows the mean and standard deviation of rain rate in mm/hr during the first period, August 31-September 13, 1987. The pattern of mean state is comparable with the seasonal mean as determined by Prabhakara *et al.*, (1992). The distribution of rainfall is consistent with that of cloud (liquid) water content in Figure 5 as expected. Most rainfall is associated with the convection in the ITCZ and SPCZ, and three typhoons over the western

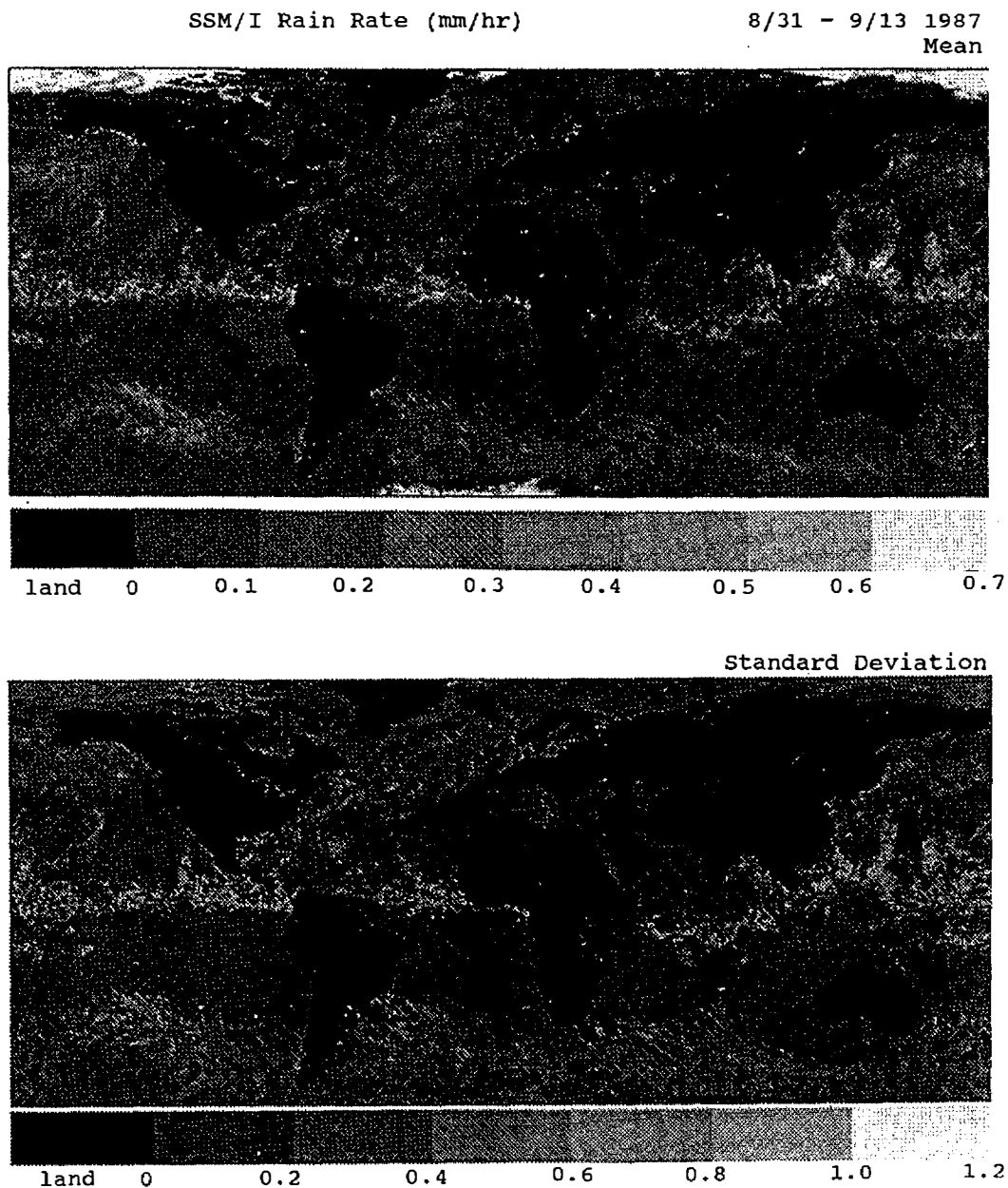


Fig. 6. Global distribution of mean and standard deviation of rain rate (mm/hr) for August 31-September 13, 1987.

Pacific Ocean. The migrating extratropical cyclones, on the other hand, do not yield large rain rate due to their transient features and weaker convection. Local maxima associated with these cyclones, however, can still be recognized in both mean and standard deviation maps. It should be also noted that difference color enhancement schemes are used in maps of mean state and standard deviation. The magnitudes of standard deviation are almost twice as large as that of mean state.

The mean and standard deviation of total precipitable water, cloud (liquid) water content, and rain rate for the second period (September 14-27) are presented in Figures 7-9. Basically they are similar to those of the first period (August 31-September 13) in pattern and magnitudes. The notable differences are the lower values over the western Pacific Ocean, and more active convection over the India Ocean. The SPCZ is also more pronounced during this period. The maximum variation of the eastern coast of Japan is possibly due to the transient features of extratropical cyclones.

SSM/I data consist of ascending and descending swaths, that represent morning passes (6:12 am crossing-equator local time) and evening passes (6:12 pm crossing-equator local time). It is of interest to investigate the diurnal variation of convection and rainfall as suggested by Albright *et al.* (1985), Hartman and Recker (1986), and Petty and Katsaros (1992). Figures 10 and 11 shows the mean rain rate of morning (upper panels) and evening (lower panels) of the first and second periods, respectively. The main features of convection are similar, but different in magnitudes. It appears to confirm a tendency toward larger areal extent and greater mean intensity of oceanic rainfall in the morning than in the evening, over much of the world's oceans. This finding is consistent with other research (e.g., Petty and Katsaros, 1992).

## 5. Brightness temperatures of typhoons

The full resolution swaths (128 by 1610 pixels) of brightness temperatures of SSM/I frequencies are first chosen, if they are in the studied period of typhoons (September 4-17, 1987) and fall within the studied domain ( $9.5^{\circ}$ - $37^{\circ}$ N, and  $105^{\circ}$ - $162.5^{\circ}$ E). The daily mosaics of the ascending swaths and descending swaths are produced separately in PC-McIDAS. All the pixels values in the mosaics are converted to the VAX microcomputer for computing rain rates. Although all the frequencies of both vertical and horizontal polarization are processed, only the brightness temperatures of vertical polarization will be presented. The  $8^{\circ}$  lat. (95 lines) by  $8^{\circ}$  long. (89 elements) box centered at the center of the Typhoon is selected in the Cartesian coordinate system. The brightness temperatures in this box are used to study the intensity of the typhoons.

During the studied period (August 31-September 27, 1987), four typhoons (Gerald, Freda, Holly, and Ian) and one tropical depression (17 W) occurred over the western Pacific Ocean (Hoffman *et al.*, Annual Tropical Cyclone Report, 1987). Only the first three typhoons were studied because they were completely covered in this period (Typhoon Ian occurred during September 23-October 1, 1987). The tracks of Gerald, Freda, and Holly are shown in Figure 12.

Typhoon Gerald (September 4-19, 1987) matured within the monsoon trough, but did not detach from it. Typhoon Gerald, having a unusually large eye, moved northwestward from the east of Philippines, sweeping the south of Taiwan, then crossing over Formosa Strait, and it finally dissipated in the Fujian Province of China.

Typhoon Freda (September 4-17, 1987) was the first tropical cyclone during September and was the middle (geographically) of a three-storm situation (the other tropical cyclones being Gerald and Holly). Freda was unusual because it traversed fewer than 10 degrees of longitude, but 25 degrees of latitude.

Super Typhoon Holly (September 5-15, 1987) was the third tropical cyclone to develop from the active monsoon trough which also spawned Gerald and Freda. Freda and Holly

both followed a similar track, moving west-northwest first before recurving northward to about 35°N and then transforming into subtropical cyclones. The intensity of these typhoons represented by maximum surface wind speed in knots is shown in Figure 13. Also shown in Figure 13 are the plots of areal averages of brightness temperatures of SSM/I frequencies in vertical polarization. The difference between vertical and horizontal polarization is either linear (for 19.35 and 37 GHz) or small (for 85.5 GHz), therefore only vertical polarization is considered here.

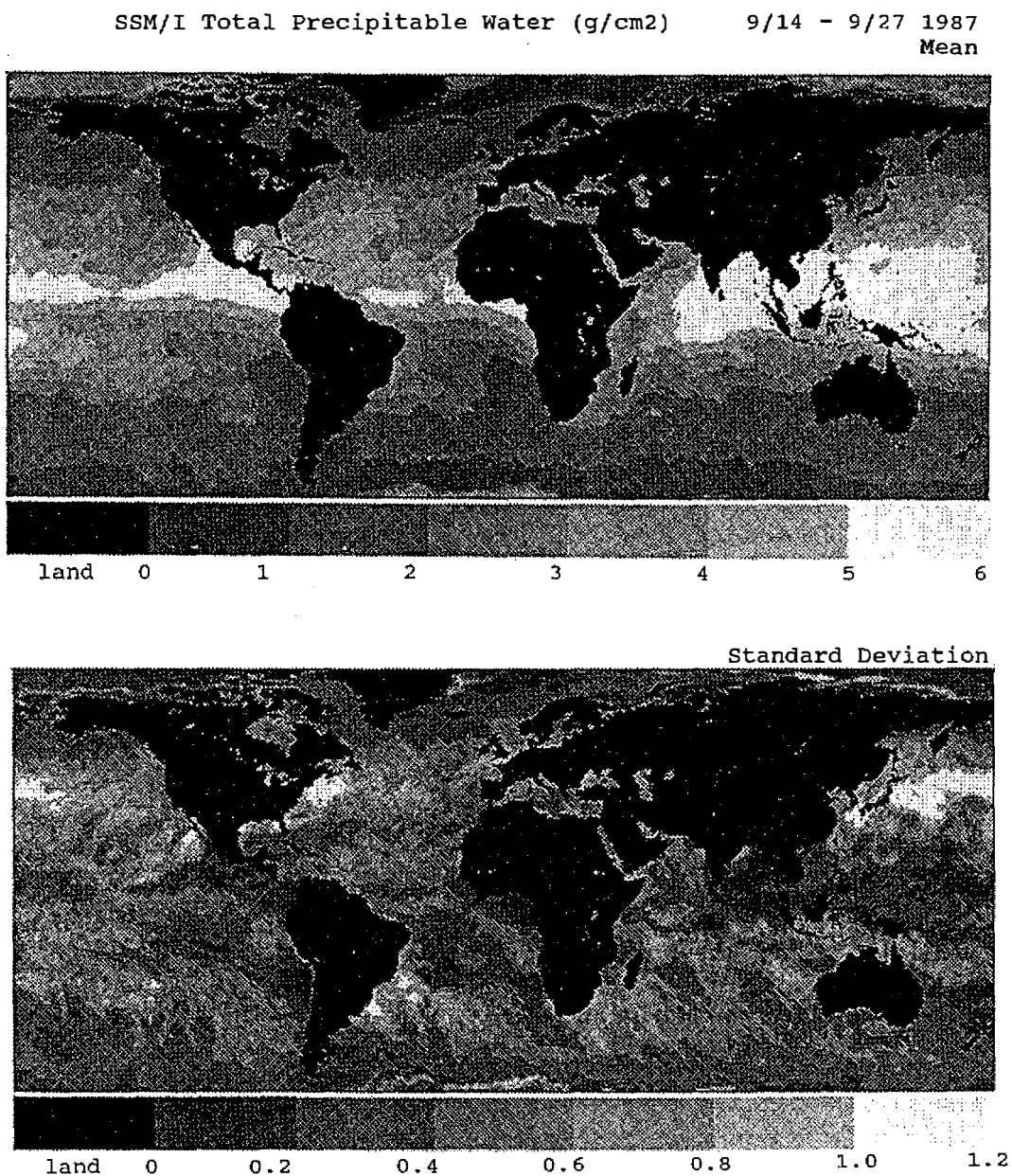
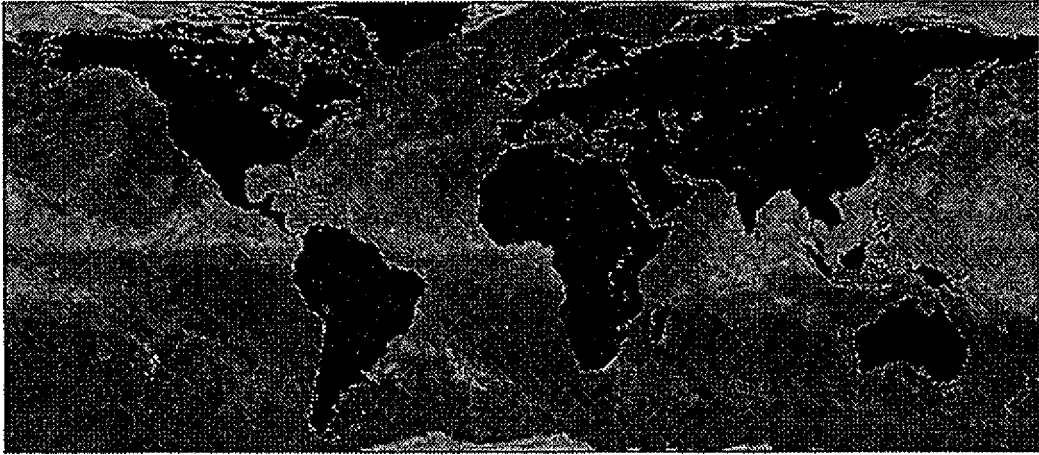


Fig. 7. Global distribution of mean and standard deviation of total precipitable water (g/cm<sup>2</sup>) for September 14-27, 1987.

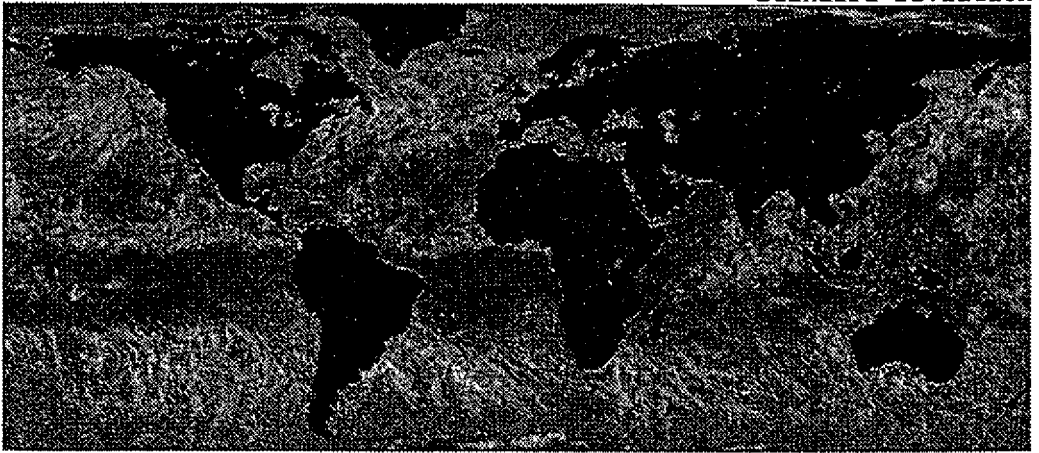
SSM/I Cloud Water Content (mg/cm<sup>2</sup>)

9/14 - 9/27 1987  
Mean



land 0 10 20 30 40 50 60 70

Standard Deviation



land 0 10 20 30 40 50 60

Fig. 8. Global distribution of mean and standard deviation of cloud water content (mg/cm<sup>2</sup>) for September 14-27, 1987.

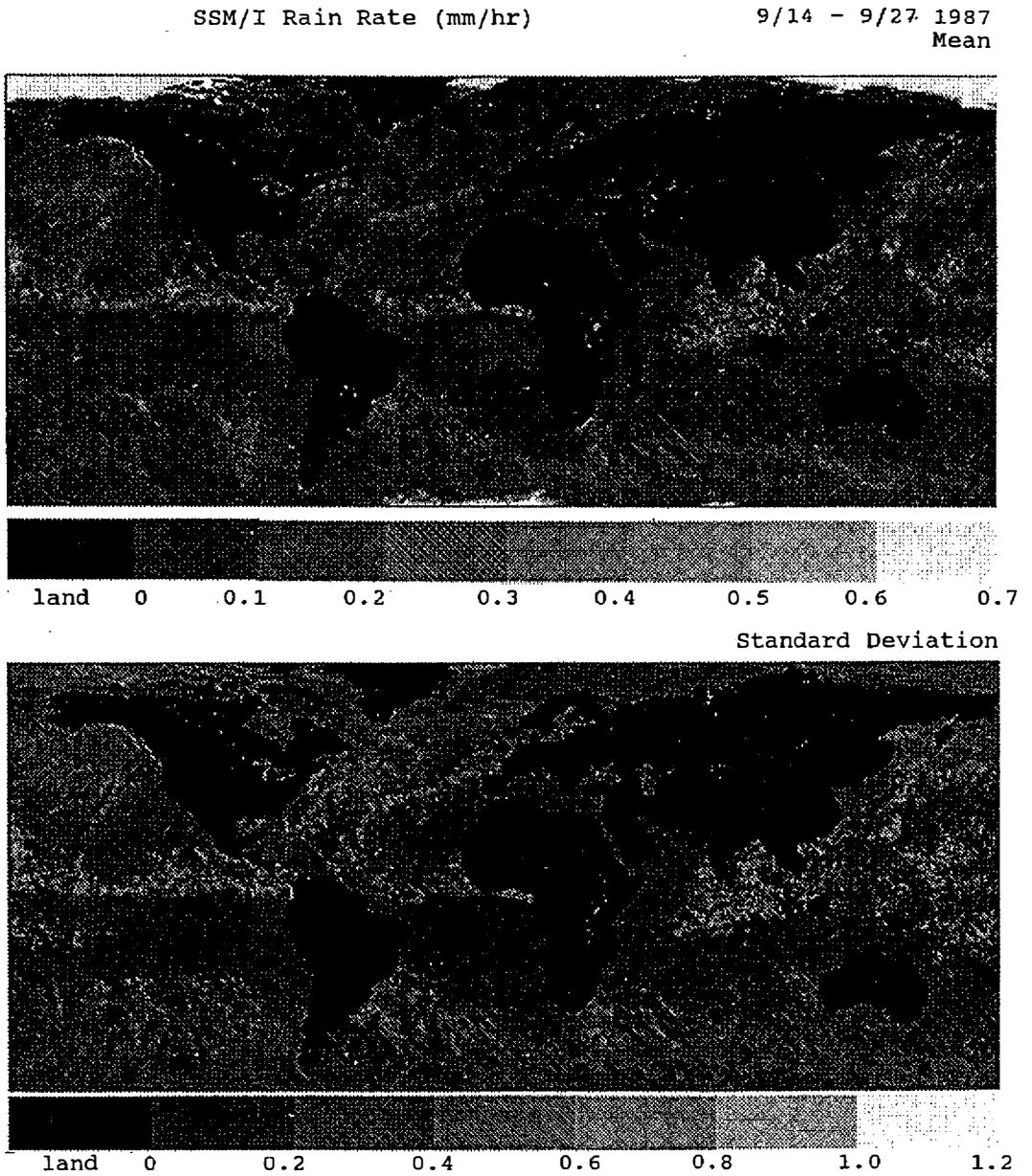
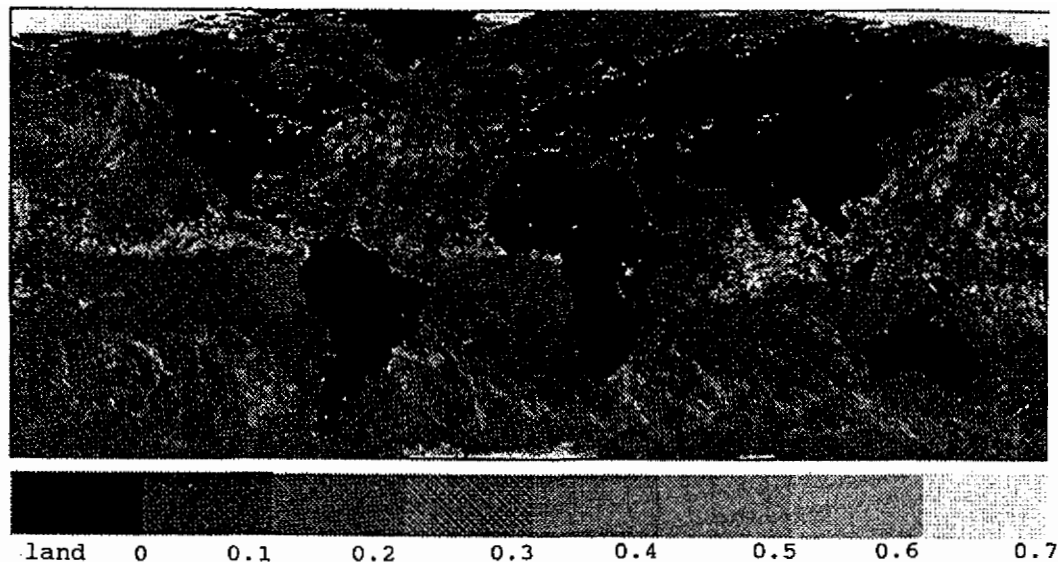


Fig. 9. Global distribution of mean and standard deviation of rain rate (mm/hr) for September 14-27, 1987.

SSM/I Rain Rate (mm/hr)

8/31 - 9/13 1987  
Mean(Ascending)

Mean(Descending)

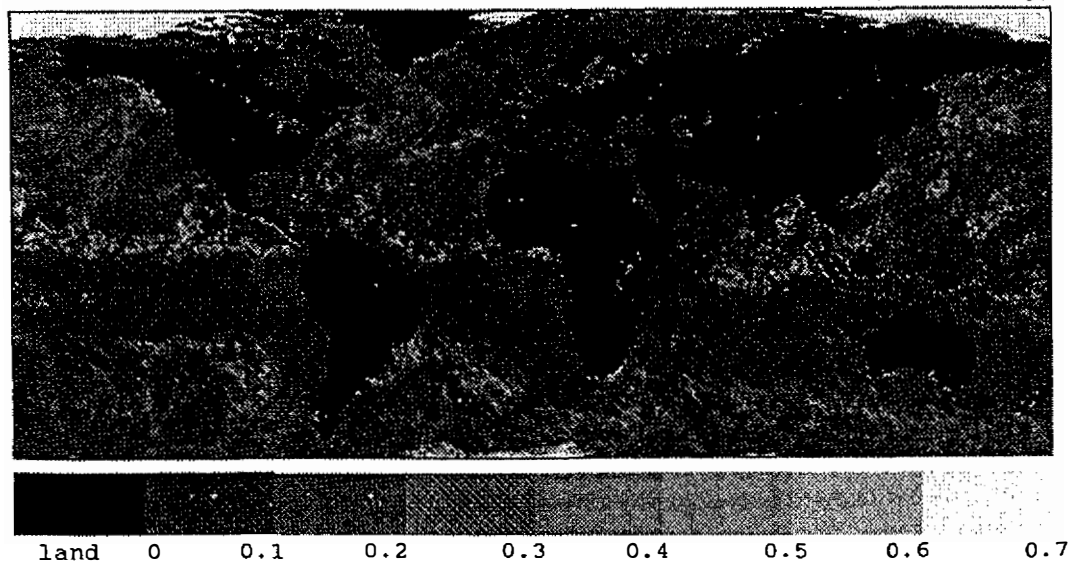


Fig. 10. Global distribution of mean of rain rate (mm/hr) from ascending swaths (morning passes, upper panel) and descending swaths (evening passes, lower panel) of August 31-September 13, 1987.

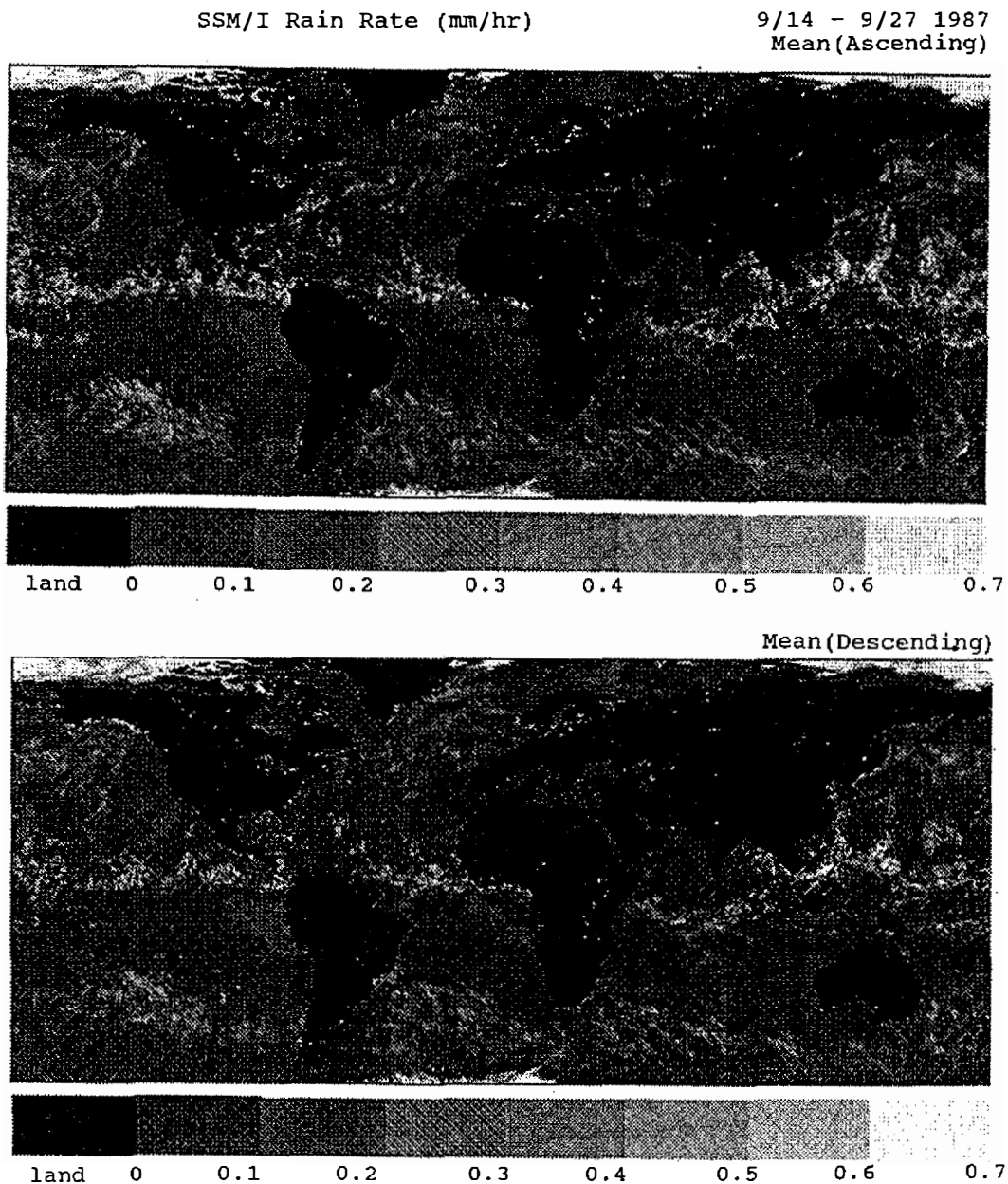


Fig. 11. Global distribution of mean of rain rate (mm/hr) from ascending swaths (morning passes, upper panel) and descending swaths (evening passes, lower panel) of September 14-27, 1987.

Typhoon Freda 18 UTC 9/4 - 00 UTC 9/17 1987  
 Typhoon Holly 18 UTC 9/4 - 12 UTC 9/10 1987  
 Typhoon Gerald 06 UTC 9/5 - 18 UTC 9/15 1987

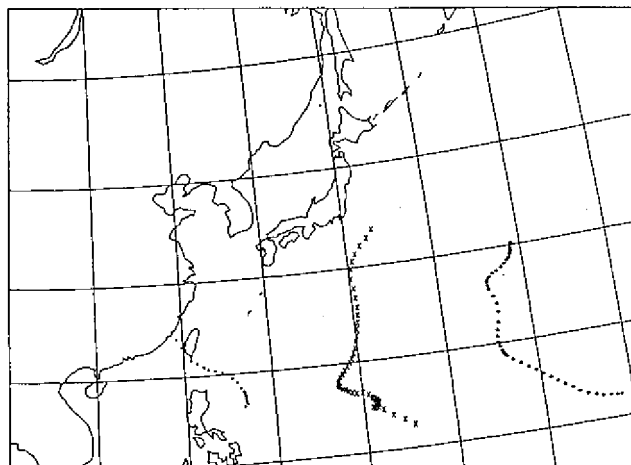


Fig. 12. Storm tracks of Typhoons Gerald (left), Freda (middle), and Holly (right).

The area is  $8^\circ$  latitudes by  $8^\circ$  longitudes box centered at the center of the typhoon. It encompasses eye, eye wall, most rain bands, and the environment of a typhoon. The area-averaged brightness temperature should reflect the changes of the structure and intensity of the typhoon. However, if the typhoon is too large and/or asymmetric, this  $8^\circ$  latitudes by  $8^\circ$  longitudes area may not be adequate to cover all the main features of a typhoon; consequently the results may be biased. Therefore the general conclusion should be inferred with caution.

The responses of 19.35 and 37 GHz are almost identical, while 19.35 GHz shows lower brightness temperatures, because it does not respond to the presence of liquid water in the clouds and water vapor in the atmosphere. The 22.235 GHz has high brightness temperatures due to the emission of microwave energy from the abundant water vapor within and near the typhoon. These brightness temperatures do not vary much and show little relationship with the intensity of the typhoon.

At 85.5 GHz, the presence of scattering of precipitation ice particles produces lower brightness temperatures as discussed in Section 2. The areal averages of 85.5 GHz brightness temperatures respond to the changes of intensity of typhoons. It appears that higher values of brightness temperature correspond to the weaker period of typhoon, the lower values to the intensifying period. This relationship is best illustrated in Typhoon Freda for its extensive coverage by the SSM/I.

However, more cases are needed to confirm this relationship, and different radii may be explored for best representation of the typhoon's features. The method of defining a threshold or using a percentage of convection in the chosen area may prove to be effective in studying the variation of intensity of a typhoon.

The cross sections of brightness temperatures at SSM/I frequencies for typhoons at the chosen times are shown in Figures 14-16. At 1003 UTC September 8, 1987, intensifying Typhoon Gerald was about 120 km to the southeast of Taiwan; most convection occurred in

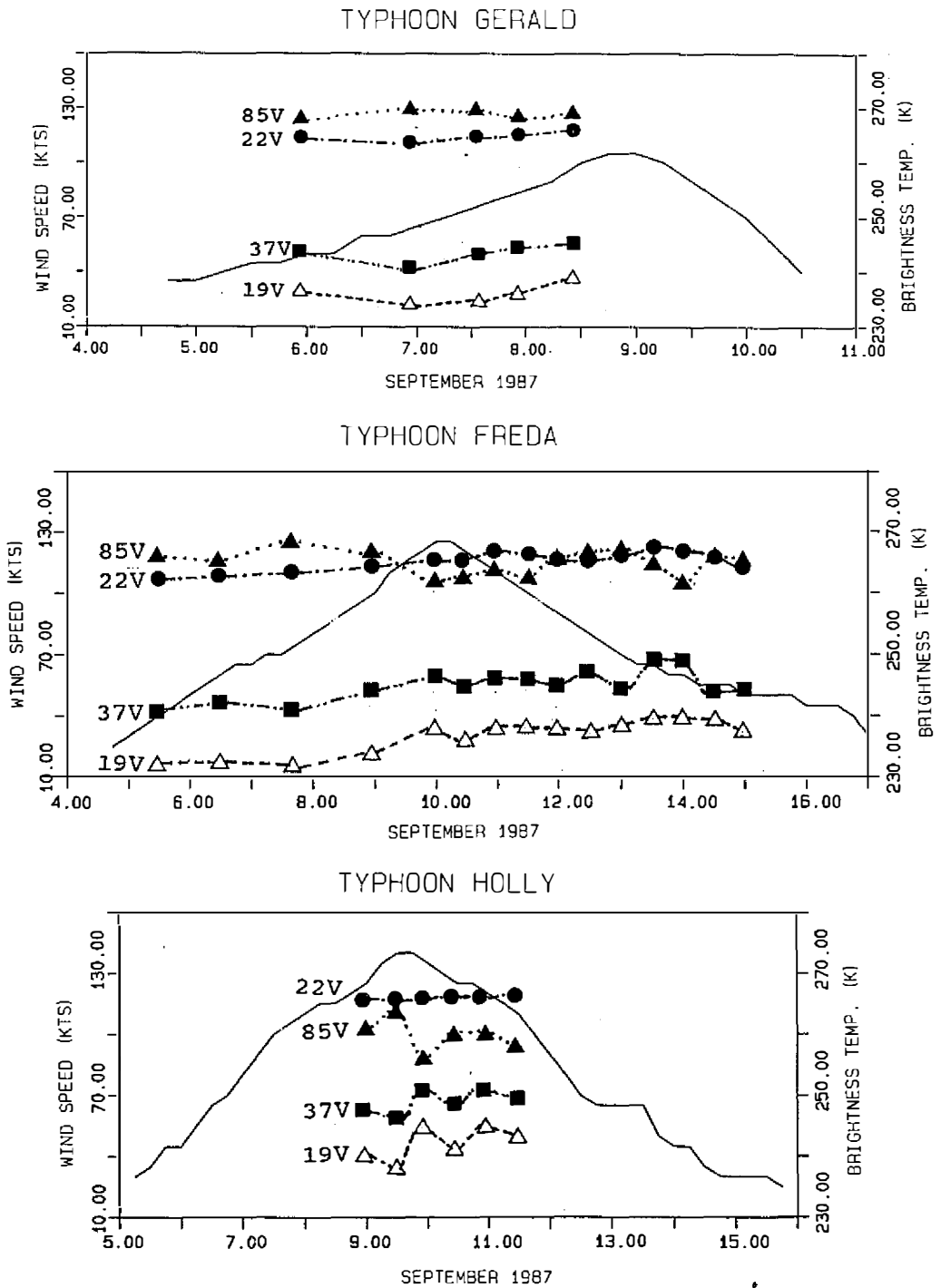


Fig. 13. Intensities and areal averages of brightness temperatures at SSM/I frequencies of Typhoons Gerald (upper panel), Freda (middle panel), and Holly (lower panel).

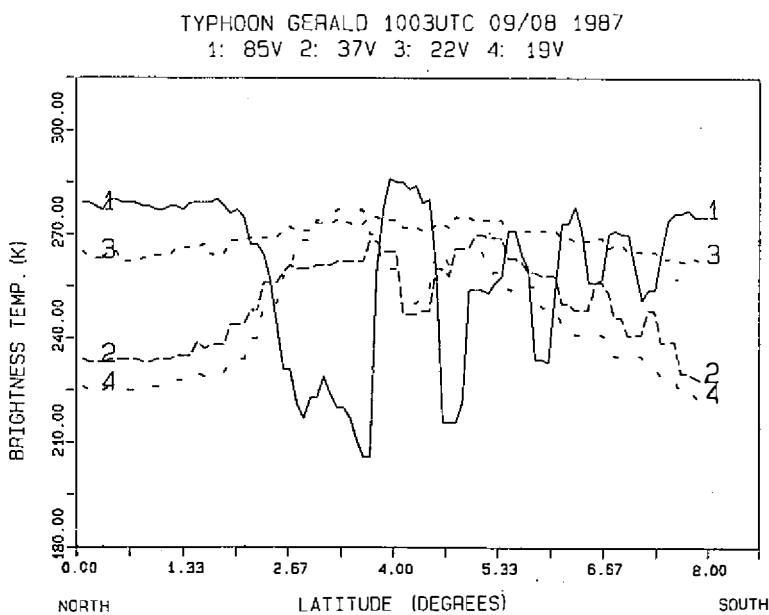
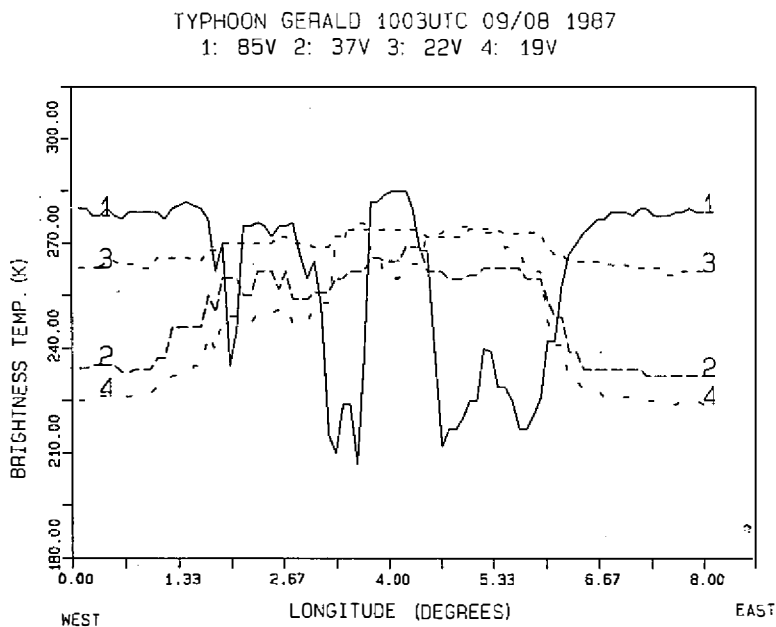


Fig. 14. East-west (upper panel) and north-south (lower panel) cross sections of brightness temperatures of Typhoon Gerald at 1003 UTC September 8, 1987.

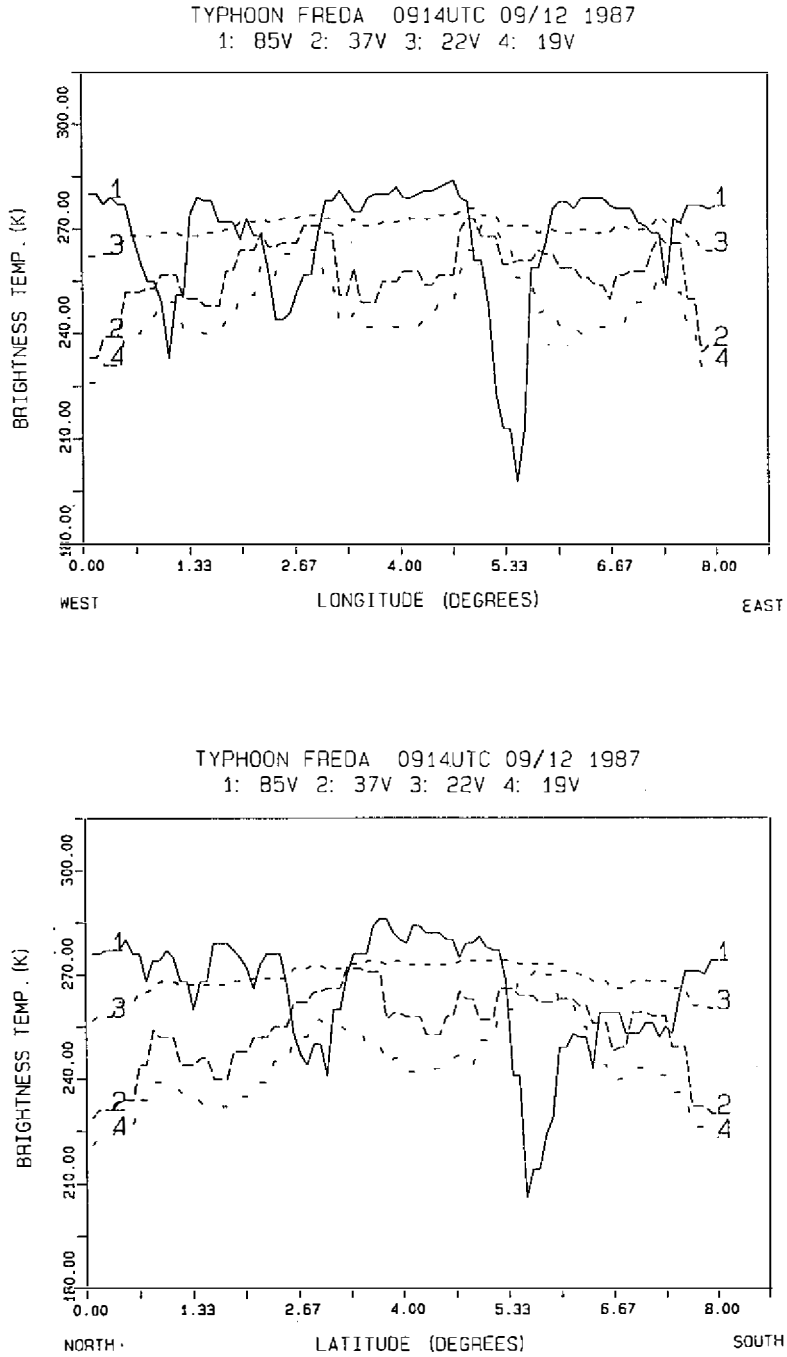


Fig. 15. East-west (upper panel) and north-south (lower panel) cross sections of brightness temperatures of Typhoon Freda at 0914 UTC September 12, 1987.

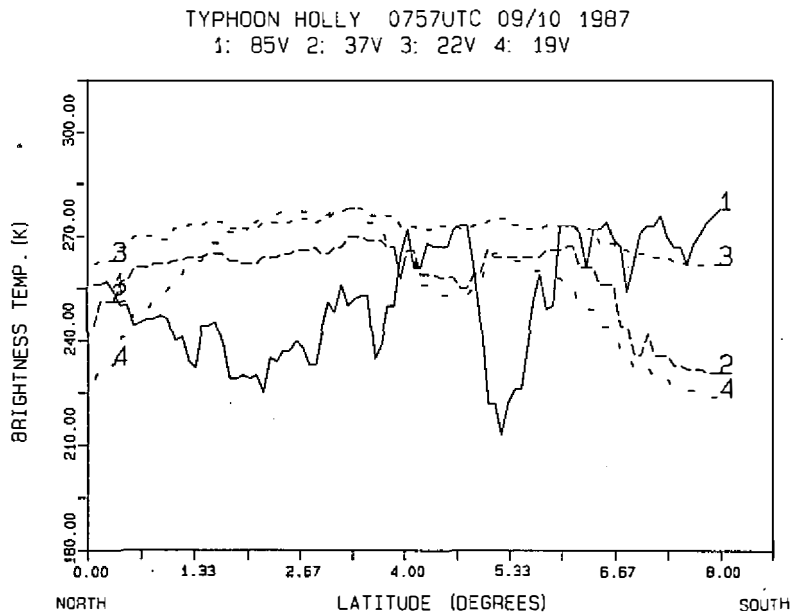
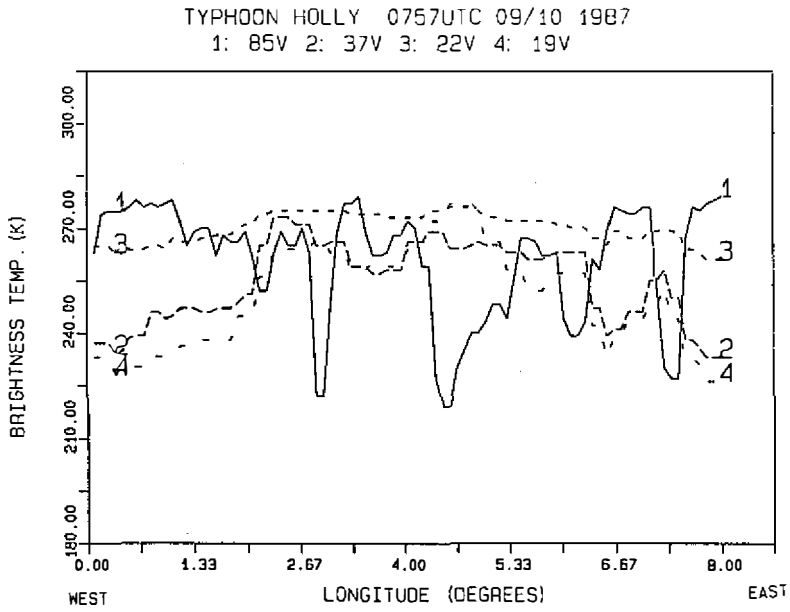


Fig. 16. East-west (upper panel) and north-south (lower panel) cross sections of brightness temperatures of Typhoon Holly at 0757 UTC September 10, 1987.

the north of the typhoon with maximum estimated rain rate being 6.5 mm/hr (see Figure 17). The surface maximum wind speed was about 95 knots.

Typhoon Gerald 1003UTC 9/8 1987 Rain Rate (mm/hr)

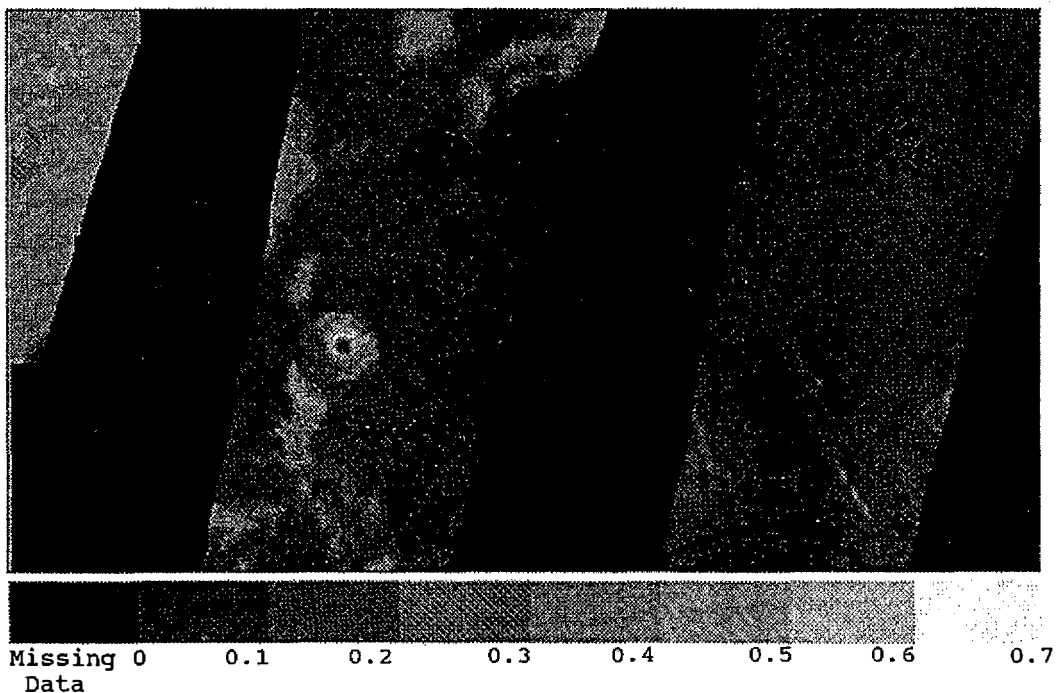


Fig. 17. Rain rate (mm/hr) of Typhoon Gerald at 1003 UTC September 8, 1987.

The east-west cross sections passing through the eye ( $4^\circ$  being the center of the typhoon) clearly show warmer than 275 K in 85.5 GHz brightness temperature at cloud-free eye. Colder temperatures at the eye wall are also noted. The responses of 19.35 and 37 GHz are similar to that of 85.5 GHz. They show moderate temperatures at the eye, warm temperatures at the rain bands, and coldest temperatures are found when farther away from the typhoon. These variations are out of phase with that of 85.5 GHz. It shows the feasibility of applying 19.35 and 37 GHz data for rainfall/convection detection as proposed by Spencer (1986), Alishouse *et al.* (1990), and Prabhakara *et al.* (1992). The 22.235 GHz data show a pattern of minimum variations at about 268 K. Since it is at the water vapor absorption line, the emission of water vapor produces higher brightness temperatures. The extensive and active convection to the north of eye is identified in the north-south cross section of 85.5 GHz data, while weaker but repeated convection is found to the south of the eye.

Weakening Typhoon Freda at 0914 UTC September 12, 1987 was at about  $19.5^\circ\text{N}$  and  $138.5^\circ\text{E}$  with moderate rain occurring to the southwest of the eye (see Figure 18). Figure 15 shows that a large eye (about 85 km in diameter) is identified by the warm brightness temperatures region at 85.5 GHz between  $3.2^\circ$  and  $5.0^\circ$  ( $4^\circ$  being the center of the typhoon). The convection to the east and south of the eye is noted for its low brightness temperatures at 85.5 GHz.

Typhoon Freda 0914UTC 9/12 1987 Rain Rate (mm/hr)

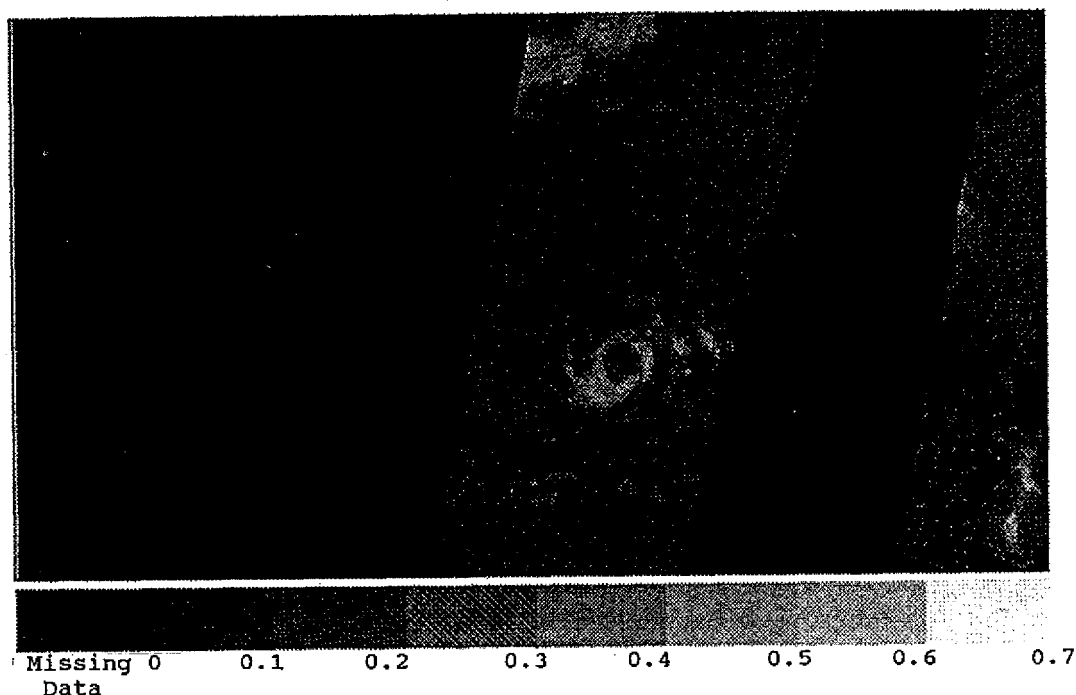


Fig. 18. Rain rate (mm/hr) of Typhoon Freda at 0914 UTC September 12, 1987.

The cross sections of Typhoon Holly at 0757 UTC September 10, 1987 is presented in Figure 16. Holly was at about  $20^{\circ}\text{N}$  and  $155.5^{\circ}\text{E}$  with extensive rainfall to the north of the eye (see Figure 19). The maximum surface wind speed was about 130 knots. The lower brightness temperatures of 85.5 GHz at eye wall are noted as expected. The symmetric structure in the east-west cross section is recognized, while more convection is found to the east of the eye.

## 6. RAINFALL ESTIMATES OF TYPHOONS

The inference of rainfall properties such as intensity and areal extent are very important to the understanding of global and regional hydrological cycle and water budget. Direct rainfall observations can be taken over the land and coastal areas, islands, and by ships. Oceanic rainfall has to be determined from the remote sensing data. Useful results have been obtained from visible and/or infrared radiometers although these instruments do not directly sense the precipitation (e.g., Kilonsky and Ramage, 1975; Arkin, 1979; Adler and Negri, 1988).

Microwave radiation can detect the presence of liquid water and precipitation ice in the clouds, so it can be applied for rainfall estimation as suggested by Wilheit *et al.* (1976), Weinman and Guetter (1977), and others.

Typhoon Holly 0757UTC 9/10 1987 Rain Rate (mm/hr)

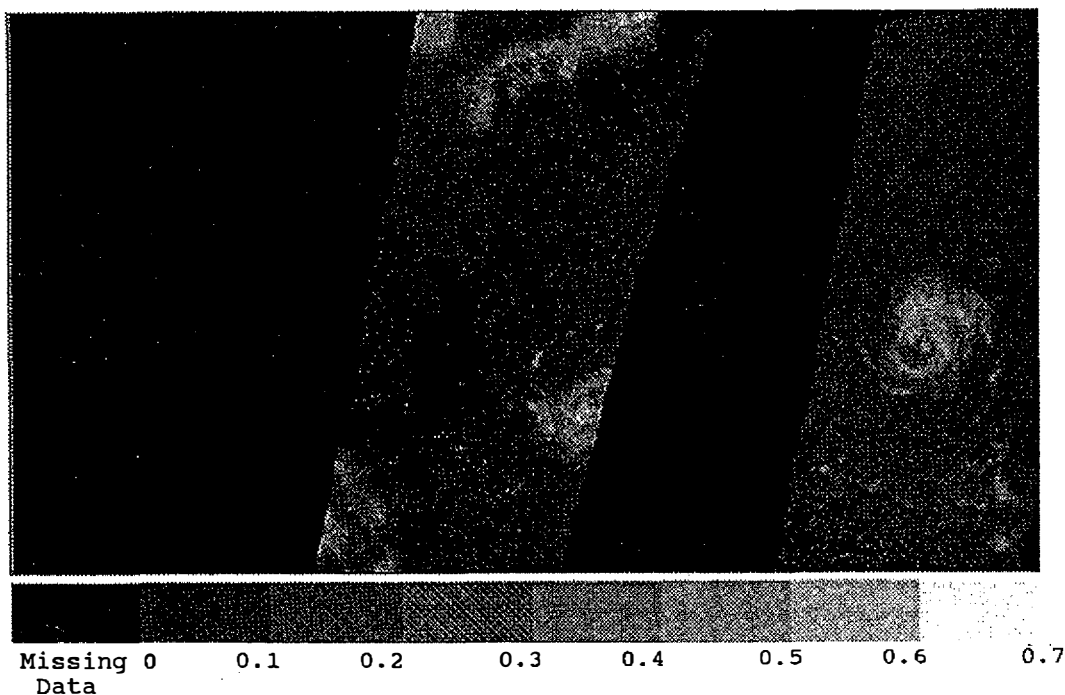


Fig. 19. Rain rate (mm/hr) of Typhoon Holly at 0757 UTC September 10, 1987.

The Nimbus-7 SMMR launched in 1978 has produced useful data for more than ten years. Using an algorithm described in Wilheit and Chang (1980), Gloersen *et al.* (1984) found reasonable agreement between coastal rain gage observations and SMMR determinations. Spencer *et al.* (1983) regressed SMMR radiances versus radar-derived rainfall rates over the Gulf of Mexico. Although a statistical regression of horizontally-polarized 37 GHz radiances against rainfall rates yielded a 72% explained variances for maritime rainfall rates, the data base was small, and no tropical cyclone data were included. Spencer and his co-investigators also concluded that a significant problem for determining rain rates for microwave radiometers was "beam filling", i.e., the instantaneous field-of-view was not uniformly filled with precipitation.

Spencer (1986) later used SMMR 37 GHz channels in both polarizations to obtain estimates of rainfall rate in Gulf of Mexico and South Atlantic precipitation systems. Prabhakara *et al.* (1992) utilized the lower SMMR frequencies (6.6 and 10.7 GHz) to estimate global distributions of total cloud water contents in precipitating clouds over the oceans. Total cloud content was then empirically related to rainfall rate.

Olsón (1987, 1991) investigated rain rate determinations for tropical cyclones. As part of that investigation radar data were used as input to a radiative transfer model which computed brightness temperatures for the SMMR frequencies and antenna patterns. Olsón then retrieved fractional beam filling from these synthetic brightness temperatures.

Recently a simplified signal channel emission-based algorithm for unpolarized 19 GHz measurements was developed by Smith and Mugnai (1988). A scattering-based algorithm of Spencer *et al.* (1989) utilizes polarization differences at 37 GHz to measure the depolarizing effects of scattering by precipitation in terms of a polarization corrected brightness temperature (PCT), from which rainfall rates were then inferred. Alishouse *et al.* (1990) empirically derived equations for predicting radar reflectivity and fraction of the field-of-view of a microwave radiometer that is filled with rain. Oceanic rainfall then is inferred from the radar reflectivity. Their results for Hurricane David show that they can explain about 2/3 of the variance in predicting the radar reflectivity. Olsón's (1991) method is based on the statistical regression of transformed brightness temperature parameters involving all four SSM/I frequencies to radar-retrieved rainfall data. Kummerow *et al.* (1991) utilizes the inversion of hydrometeor profile relationships to retrieved rainfall rates. Prabhakara *et al.* (1992) estimated oceanic rainfall from SMMR and SSM/I 37 GHz data by empirically developing a statistical relationship between the observed brightness temperatures at 37 GHz and rain rates.

In the present study, a simple algorithm is applied to estimate rain rates from the measured SSM/I brightness temperature. The algorithm was developed by Olsón (1987), and was discussed in more detail in Olsón *et al.* (1990). The algorithm, which relates brightness temperatures to the rain rate, is written as Equation(1).

$$\begin{aligned} \text{Rainrate}(mm/hr) = & \{ \exp(3.06231 - 0.0056036 \times TB(85GHzV) \\ & + 0.0029478 \times (85GHzH) - 0.0018119 \times \\ & TB(37GHzV) - 0.00750 \times TB(22GHzV) + \\ & 0.009755 \times TB(19GHzV) - 8.0 \} (1) \end{aligned}$$

The estimated rain rate for the typhoons at the selected times are depicted in Figs. 17-19. The rain rates appear to be reasonable in the vicinity of typhoons for all studied cases. The little or no rain areas are found at the eye and between rain bands, which can be identified clearly. The maximum rain rate is more than 6 mm/hr, which is comparable to the other investigations (Rao and Hutchison, 1992).

Because this algorithm can only be applied over the oceans, the rain rates over the land are not correct. It should also be noted that this algorithm tends to produce small rain rates (less than 1 mm/hr) over cloudfree regions. In the present study, the pattern and relative intensity of rainfall are more emphasized than the accuracy of absolute values. The validation of the algorithm is needed, but there are only sporadic surface and upper observations over the oceans. The intercomparisons of various rainfall algorithms based on different theories seem to be feasible.

## 7. CONCLUDING REMARKS

Microwave data such as SSM/I provides unprecedented opportunity to study global aspects of moisture. The hydrological variables as estimated by the SSM/I are crucial for global water budget. The results of using passive microwave measurements can also be useful for the verification of numerical model outputs.

The SSM/I data could provide realistic patterns and magnitudes of total precipitable water, cloud water content, and rain rate for the globe. They are comparable to the previous findings and other model analysis. The characteristics of SSM/I data are documented in

this study for the three typhoons (Gerald, Freda, and Holly) over the western Pacific Ocean. The detailed structure of the typhoon can be identified by the SSM/I data, and the estimated rainfall of the typhoon appears to be reasonable.

It is recognized that the quantitative comparison between SSM/I rainfall estimation and ground truth observation is essential and urgently needed. The development of specialized algorithms for Taiwan area is suggested, and it requires efforts of collecting long term surface, upper air and radar data. The incorporation of cloud and radiation transfer models should be utilized in developing the algorithms. The intercomparisons of various algorithms can also be performed, if ground truth data are not available.

**Acknowledgements** The first author thanks his colleagues at the Center for Space and Remote Sensing Research for their generous help in facility support.

We are also indebted to Mr. Kwang-Hwa Wang for his help in computing and programming.

Our special thanks also go to NASA/MSFC (Marshall Space Flight Center) WetNet user group, which produced and provided DMSP SSM/I image data for this study. This project is supported under the Visiting Scientist Program of National Science Council (NSC); the contract number is NSC 81-0202-M-008-543.

## REFERENCES

- Adler, R. F., and A. J. Negri, 1988: A satellite infrared technique to estimate tropical convective and stratiform rainfall. *J. Appl. Meteor.*, **27**, 30-51.
- Adler, R.F., W.K. Tao, N. Prasad, J. Simpson, and H. Y., Yeh, 1988: Satellite microwave rainfall simulations with a three-dimensional dynamical cloud model. Preprint of the Third Conference on Satellite Meteorology and Oceanography. Boston, American Meteorological Society, 290-295.
- Albright, M. D., E. E. Recker, R. J., Reed, and R. Dang, 1985: The diurnal variation of deep convection and inferred precipitation in the Central Tropical Pacific during January-February 1979. *Mon. Wea. Rev.* **113**, 1662-1680.
- Alishouse, J. C., 1983: Total precipitable water measurements from the Seasat Scanning Multichannel Microwave Radiometer. *J. Geophys. Res.*, **83**, 1929-1935.
- Alishouse J. C., R. R. Ferraro, and J. V. Fiore, 1990: Inference of oceanic rainfall properties from the Nimbus 7 SMMR. *J. Appl. Meteor.*, **29**, 551-560.
- Arkin, P. A., 1979: Relationship between fractional coverage of high cloud and rainfall accumulations during GATE over "B" scale array. *Mon. Wea. Rev.*, **107**, 1382-1387.
- Gloerson, O., D. J. Cavalieri, A. T. C. Chang, T.T. Wilheit, W. J. Campbell, O. M. Johannessen, K. B. Katsaros, K. F. Kunzi, D. B. Ross, D. Stalin, E. P. L. Windsor, F. T. Barath, P. Gudmandsen, E. Langham, and R. O. Ramsier, 1984: A summary of results from the first Nimbus 7 SMMR observations. *J. Geophys. Res.*, **89**, 5335-5344.
- Hakarinen, I. M., and R. F. Adler, 1988: Observations of precipitation convective systems at 92 and 182 GHz. *Meteor. Atmos. Phys.*, **38**, 164-182.
- Hartmann, D. L., and E. E. Recker, 1986: Diurnal variation of outgoing longwave radiation in the tropics. *J. Climate Appl. Meteor.*, **25**, 800-812.

- Heysfield, G. M., and R. Fulton, 1988: Comparison of high altitude remote aircraft measurements with the radar structure of an Oklahoma thunderstorm: Implications for precipitation estimation from space. *Mon. Wea. Rev.*, **116**, 1157-1174.
- Hoffman, C. W., V.G. Patterson, and D.J. McMorro, 1987: 1987 Annual Tropical Cyclone Report. U. S. Naval Oceanography Command Center/Joint Typhoon Warning Center, Comnavmar Box 17, FPO San Francisco, CA.
- Hollinger, J., R. Lo, G. Poe, R. Savage, and J. Peirce, 1987: Special Sensor Microwave/Imager User's Guide. Washington, D.C., Naval Research Laboratory.
- Huang, H.-J., and G.-R. Liu, 1992: Western Pacific Moisture Analysis as Observed from DMSP SSM/I Measurements. Final report of NSC contract 81-0202- M-008-543, 63 pp.
- Kilonsky, B. J., and C. S. Ramage, 1975: A technique for estimating tropical open ocean rainfall from satellite observations. *J. Appl. Meteor.*, **15**, 972-975.
- Kummerow, C., I. M. Hakkarinen, H. F. Pierce, and J. A. Weinman, 1991: Determination of precipitation profiles from airborne passive microwave radiometric measurements. *J. Atm. Oceanic Tech.*, **8**, 148-158.
- Olsón, W. S., 1987: Estimation of rainfall rates in tropical cyclones by passive microwave radiometry. Ph. D. Thesis. University of Wisconsin, Madison, WI, 292 pp.
- Olsón, W. S., 1991: The use of WetNet as a tool for precipitation algorithm intercomparisons, browse algorithms, and PC library of algorithms for recalculation, validation, and algorithm integration. Presented at WetNet Science and Analysis Colloq., UCSB, Santa Barbara, CA, 19-22 February 1991.
- Olsón, W. S., F. J. Fontaine, W. L. Smith, and R. H. Achtor, 1990: Recommended algorithms of the retrieval of rainfall rates in the tropics using SSM/I (DMSP F8). Manuscript, University of Wisconsin, Madison, WI, 10 pp.
- Petty, G. W., and K. B. Katsaros, 1992: Morning-evening differences in global and regional oceanic precipitation as observed by the SSM/I. Preprint of the Sixth Conference on Satellite Meteorology and Oceanography, Atlanta, GA, January 5-10, 1992, 282-285.
- Prabhakara, C., G. Dalu, G. L. Liberti, J. J. Nucciarone, and R. Suhasini, 1992: Rainfall estimation over oceans from SMMR and SSM/I microwave data. *J. Appl. Meteor.*, **31**, 532-552.
- Rao, P. K., S. J. Holmes, R. K. Anderson, J. S. Winston, P. E. Lehr, 1990: Weather satellites: Systems, data, and environmental applications. American Meteorological Society, Boston, MA, 503 pp.
- Rao, G. V., and T. D. Hutchison, 1992: The SSM/I derived total rainfall amounts of typhoons and the possible relationship between rain rates and SST's. Preprint of the Sixth Conference on Satellite Meteorology and Oceanography, Atlanta, GA, January 5-10, 1992, 282- 285.
- Smith, E. A., and A. Mugnai, 1988: Radiative transfer to space through a precipitating cloud at multiple microwave frequencies. Part II: Results and analysis. *J. Appl. Meteor.*, **27**, 1074-1091.
- Spencer, R. W., 1986: A satellite passive 37 GHz scattering-based method for measuring oceanic rain rates. *J. Climate Appl. Meteor.*, **25**, 754-766.

- Spencer, R. W., B. B. Hinton, and W. S. Olsón, 1983: Nimbus 7 37 GHz radiances correlated with radar rain rated over the Gulf of Mexico. *J. Climate Appl. Meteor.*, **22**, 2095-2099.
- Spencer, R. W., H. M. Goodman, and R. Hood, 1989: Precipitation retrieval over land and ocean with the SSM/I; identification and characteristics of the scattering signal. *J. Atm. Oceanic Tech.*, **6**, 254-273.
- Weinman, J. A., and P. J. Guetter, 1977: Determinations of rainfall distributions from microwave radiation measured by the Nimbus 6 ESMR. *J. Appl. Meteor.*, **16**, 437-442.
- Wilheit, T. T., and A. T. C. Chang, 1980: An algorithm for the retrieval of ocean surface and atmospheric parameters from the observations of the SMMR. *Radio Sci.*, **15**, 525-544.
- Wilheit, T. T., J. S. Theon, W.E. Shenk, L. J. Allison, and E. B. Rodgers, 1976: Meteorological interpretations of the images from the Nimbus 5 Electrically Scanned Microwave Radiometer. *J. Appl. Meteor.*, **15**, 166-172.
- Wilheit, T. T., J. L. King, E. B. Rodgers, R. A. Nieman, B. M. Krupp, A. S. Milman, J. S. Stratigos, and H. Siddalingaiah, 1982: Microwave radiometric observations near 19.35, 35, 92 and 183 GHz of precipitation in tropical storm Cora. *J. Appl. Meteor.*, **21**, 1137-1145.
- Wu, R., and J. A. Weinman, 1984: Microwave radiances from precipitating clouds containing aspherical ice, combined phase, and liquid hydrometeors. *J. Appl. Res.*, **89**, 7170-7178.

# 由DMSP SSM/I資料探討西太平洋水汽含量之分佈

黃火金<sup>1</sup>, 劉振榮<sup>2</sup>, 林唐煌<sup>2</sup>

1. 美國北卡羅萊納大學及  
國立中央大學太空及遙測研究中心客座副教授
2. 國立中央大學太空及遙測研究中心

## 摘要

本研究主要利用DMSP氣象衛星SSM/I資料探討全球水汽含量的分佈。並以1987年9月份颱風為對象，研究颱風強度與衛星資料亮度溫度間之關係。颱風降水量的估算則應用 Olson 等人於1990年發表之模式。

由研究結果發現，SSM/I 資料可提供全球的水汽含量、液態水含量及降水量等合理的分佈型態及大小。其估算值並與以往之研究結論和其它模式分析之結果作比較。研究中亦說明了分析西太平洋的三個颱風 (Gerald, Freda 和 Holly) 在 SSM/I 觀測資料上的特性。由 SSM/I 資料亦可辨別颱風的細微結構，而其降水量的估算則有非常合理之結果。

研究的結果顯示，可以利用 SSM/I 資料來研究發展適合臺灣及鄰近地區使用的大氣參數計算模式。模式之建立則可配合雷達觀測、高空及地面觀測資料，以增加模式之實用性。而若無地面實測資料以供模式結果之驗證，則可與其它不同模式之結果相互比較，以分析研究模式之合理性與適用性。